Full Length Article

Absolute adsorption of light hydrocarbons and carbon dioxide in shale rock and isolated kerogen

Tianhao Wu[a,1], Huangjing Zhao[a,1], Stéphane Tesson[a,b], Abbas Firoozabadi[a,*]

[a] *Reservoir Engineering Research Institute, 595 Lytton Avenue Suite B, Palo Alto, CA 94301, USA*
[b] *Department of Chemical and Environmental Engineering, Riverside, CA 92521, USA*

ABSTRACT

Natural gas production from shale formations has changed the energy landscape. Knowledge of adsorption in the subsurface shale formations improves resource assessment. The excess adsorption is directly measurable from experiments. Evaluation of fluid content in shale is based on the absolute adsorption. At high pressure relevant to subsurface conditions, the computation of absolute adsorption from excess adsorption has shortcomings when the conventional models are used. In this work, we first present the excess sorption data of light hydrocarbons and carbon dioxide in subsurface shale rock and in isolated kerogen. Gravimetric method was used in our measurements. The results show that, at high pressure, the excess adsorption of ethane and carbon dioxide decreases significantly as pressure increases. Excess adsorption of ethane at 60 °C for the shale sample investigated becomes negative at high pressure. The conventional models may provide a non-monotonic absolute adsorption and even magnify the unphysical negative adsorption. In addition to the proposed model based on adsorbed layer volume, we also account for effective sample volume due to the pore volume accessibility by different molecules, as well as the swelling of kerogen. The adsorption data from subsurface shale and the method for analysis presented in this work set the stage for prediction capability in hydrocarbon production from shale reservoirs.

1. Introduction

Production of natural gas, a clean-burning fuel, from shale formations has changed the energy landscape in the last few years. Fracturing of tight shale formations, flow in the shale subsurface, and fluid content in the formation are the key elements. This investigation focuses on the absolute adsorption which has significant effect on fluid content in shale formations. Knowledge of adsorption is important in shale oil and gas reservoirs for resource assessment. Shale rock is comprised of two distinct media: organic and inorganic matters, both may contain nanoscale pores [1]. Generally, kerogen is the predominant component of organic matter in most shale formations. The amount of hydrocarbons in shale is often associated with organic matter [2–4].

There are two main methods for measuring gas adsorption: gravimetric and manometric/volumetric [5]. The excess adsorption is directly measured in experiments. The absolute adsorption can be estimated based on excess adsorption. Much work has been done in various experimental measurements of excess adsorption. However, the calculation of absolute adsorption from excess adsorption in shale has not

advanced much. The main reason may be that at low and moderate pressures the absolute adsorption and excess adsorption are close. The absolute adsorption of methane and/or carbon dioxide in various shale samples has been investigated based on the conventional models where the main parameter is the adsorbed layer density [2,6–11]. The absolute adsorption can also be estimated based on the adsorbed layer volume [12–14].

Negative excess adsorption has been reported in different materials. Gasparik et al. [15] reported extensive excess adsorption measurements in shale by gravimetric and volumetric methods and discussed the uncertainty in measurements. They presented negative excess adsorption of carbon dioxide in Posidonia shale and reasoned that the negative data is due to the deviation from bulk fluid density calculation and cross-contamination of the carbon dioxide with residual helium. The negative excess adsorption of methane has been reported by Ross and Bustin [16]. The authors believed that negative excess adsorption was due to the error of void volume calibration from the different pore-space accessibility by helium and methane. Helium can access small pores where the larger molecules may not access. Negative excess

---

* Corresponding author.
 E-mail address: af@rerinst.org (A. Firoozabadi).
[1] These authors contributed to the work equally and should be regarded as co-first authors.

adsorption of carbon dioxide in coal has also been reported [17]. As we will show in this work an alternative explanation is warranted.

In general, the fluid-in-place (FIP) in shale rock can be divided into three categories: free molecules in the pores; adsorbed species on the inner surfaces of the microscale and nanoscale pores; and dissolved species in the organic matter [18]. The former two categories may have major contribution to the total FIP [4,10,19]. Kerogen may swell due to complex mechanisms, such as structural trapping, adsorption, and dissolution. A number of authors have studied shale/kerogen swelling by organic solvents including aliphatic, alicyclic and aromatic hydrocarbons [20–25]. Kerogens are cross-linked macromolecular systems. Regular solution theory has been used to describe the solvent swelling of kerogens [22]. Heller and Zoback [6] studied the volumetric swelling as a function of methane and carbon dioxide adsorption in activated carbon, illite, and kaolinite. They observed increased swelling when the amount of adsorption increased. The volumetric swelling with slight anisotropy due to methane adsorption has been reported in other studies [19]. Yang et al. [26] have done sensitivity analysis on the effect of shale swelling and shrinkage as wells adsorbed phase volume and excess adsorption and absolute adsorption from methane in several shale samples. The assumptions in their work include a constant adsorbed density and variable adsorb phase volume which are different from our work.

In this work, we first report excess adsorption/desorption data and then propose a model for absolute adsorption estimation from measured excess adsorption. We estimate absolute adsorption based on adsorbed layer volume, and the effects of pore volume accessibility and effective sample volume, as well as swelling. Our data is based on the gravimetric method in reservoir shale samples and the isolated kerogen for methane, ethane, propane, *normal*-butane (*n*-butane), *iso*-butane (*i*-butane), and carbon dioxide. The pressure in methane, ethane and carbon dioxide is to 150 bar, and the temperature ranges from 60 °C to 120 °C. For propane, *n*-butane, and *i*-butane the pressure is set by the vapor pressure at experimental temperature conditions. At the end, we draw conclusions.

2. Experimental method

2.1. Basic properties

The sorption in shale reservoir rocks from Vaca Muerta formation, Neuquén Basin in Argentina, was investigated in this study. The geological formation is Jurassic and Cretaceous age and considered to have high potential for the production of oil and gas [27]. The basic properties were analyzed systematically, including density, pore size distribution, mineral composition, organic petrography, and thermal maturity. Kerogen was isolated from the shale sample by acid treatment and Soxhlet extraction process [28]. The details and procedures of basic property tests and kerogen isolation are provided in the SI.

2.2. Gas adsorption/desorption by gravimetric method

Adsorption/desorption of various light hydrocarbons, including methane (99.97%), ethane (99%), propane (99.5%), *n*-butane (99.999%), *i*-butane (99.999%), and carbon dioxide (99.5%) in the shale and isolated kerogen were investigated using an ISOSORP® STATIC (SC-HPII) Automatic Gravimetric High Pressure Sorption Analyzer. The instrument is manufactured by RUBOTHERM. The schematic diagram of the gravimetric adsorption analyzer is presented in Fig. S1. The sorption amount is determined gravimetrically by weighing the sample using the patented magnetic suspension balance. Resolution of the magnetic suspension balance is 0.01 mg and the reproducibility is ± 0.04 mg (standard deviation).

First, the weight (m^{SC}) and volume (V^{SC}) of the empty sample container were measured with helium (99.999%) at 60 °C. This step is known as the blank measurement. Second, around 0.3 to 2.5 g of

sample was loaded to the sample container and was vacuum (ultimate vacuum with gas ballast is 0.01 mbar) dried at 200 °C until there was no weight change. This step is known as the sample pretreatment. In the third step, the weight (m^S) and the volume (V^S) of the loaded sample were determined with helium at 60 °C. V^S is the volume of the grain matrix and does not include the pore volume measured from low temperature adsorption analysis. This step is known as the buoyancy measurement. In the fourth step, the loaded sample was evacuated again at 200 °C until there was no weight change, and then the adsorption/desorption measurements were conducted. In the adsorption (desorption) measurement, the pressure of the gas was increased (decreased) stepwise at a constant temperature. After each adsorption/desorption measurement cycle, the loaded sample was reprocessed by vacuum dry at 200 °C, followed by the next adsorption/desorption measurement. Adsorption and desorption were measured at equilibrium. For each of the measuring point, the pressure and temperature were in the tolerance of ± 0.1 bar for setting pressure and ± 0.1 °C for setting temperature, respectively. Each adsorption/desorption point was measured after 0.5–3 h depending on the gas species [29].

2.3. Excess adsorption and conventional model for absolute adsorption

There are two forces acting on the sample in the gravimetric method: gravity (F_A) and buoyancy (F_B) are given by,

$$F_A = (m^{SC} + m^S + m^A)g \tag{1}$$

$$F_B = (V^{SC} + V^S + V^A)\rho^B g \tag{2}$$

where m^A is the absolute adsorption, V^A is the volume of the adsorbed layer, ρ^B is the bulk density of the fluid, and g is the gravity acceleration. Bulk density of the fluid is determined by a sinker, which has a known weight and volume. m^{SC}, V^{SC}, m^S, and V^S are obtained using helium in the blank measurement and buoyancy measurement. In sorption measurements, the balance reading, Δm, and the mass of adsorbate m^A are given by,

$$\Delta m = (F_A - F_B)/g = m^{SC} + m^S + m^A - (V^{SC} + V^S + V^A)\rho^B \tag{3}$$

$$m^A = \Delta m - m^{SC} - m^S + (V^{SC} + V^S + V^A)\rho^B \tag{4}$$

The excess adsorption can be expressed as

$$m^E = \Delta m - m^{SC} - m^S + (V^{SC} + V^S)\rho^B \tag{5}$$

Eq. (5) has the same form as m^A in Eq. (4) when $V^A = 0$. The relationship between absolute adsorption and excess adsorption can be written as

$$m^A = m^E + V^A \rho^B \tag{6}$$

The adsorbed layer volume can be expressed by,

$$V^A = \frac{m^A}{\rho^A} \tag{7}$$

where ρ^A is the average adsorbed layer density. By substituting Eq. (7) into Eq. (6), the relationship between absolute adsorption and excess adsorption can also be given as

$$m^A = \frac{m^E}{1 - \rho^B/\rho^A} \tag{8}$$

The excess adsorption is obtained from experimental measurements based on Eq. (5). The absolute adsorption can be estimated based on either Eqs. (6) or (8) [30]. In Eq. (6), because the adsorbed layer volume V^A cannot be measured directly, many assumptions have been made by various authors. Payne et al. [31] introduced the approximation based on surface area and effective adsorbed layer thickness. Rexer et al. [12] applied the sorption pore volume estimated from CO_2 isotherms at −78 °C (195.15 K) as an upper limit. Zhang et al. [13] and Tian et al. [14] estimated adsorbed layer volume based on linear

regression of the excess adsorption data at saturated condition. The total pore volume has also been used as the adsorbed layer volume when the micropores are dominant [32,33]. In Eq. (8), the adsorbed layer density is often assigned as constant. The density has also been approximated by the van der Waals constant *b* [6,34–36]. In another approximation, the adsorbed layer density is assumed to be the liquid density at normal boiling point [37–40]. The liquid density as a function of temperature has also been used [36]. Because of the ambiguity in methane adsorbed density, we have recently suggested the adsorbed layer density from molecular simulations [29]. Other expressions has also been proposed based on the constant adsorbed layer density, including Dubinin–Radushkevich model and its modifications [41].

3. Conventional model

3.1. Basic properties

The samples were pretreated at 200 °C under vacuum condition. The densities of shale and the isolated kerogen samples were measured using helium at 60 °C, the values of which are 2.633 g/cm³ and 1.720 g/cm³, respectively. The mineralogy of the shale rock is dominated by quartz, calcite, and clay (Table S1). The thermal maturity in terms of vitrinite reflectance is 0.53% for the shale sample. Surface area, pore volume, and average pore size of shale and isolated kerogen powder samples were determined by nitrogen sorption at −195.85 °C (77.3 K). Surface area was calculated using the Brunauer–Emmett–Teller (BET) model, while the pore volume and average pore size were calculated by the Barrett–Joyner–Halenda (BJH) model. The measured nitrogen sorption is presented in Fig. S2. Table S2 provides various results from nitrogen adsorption. The average pore size in the shale sample is 18.8 nm, which is lower than the value of 22.8 nm in the kerogen sample. The BET surface area and BJH pore volume in the isolated kerogen are significantly higher than in the shale sample, because of the removal of the inorganic matter and solvable organic matters.

Table S3 shows the Carbon, Hydrogen, Nitrogen, Sulfur, and Oxygen (CHNS-O) elemental analysis. The shale sample has only 3.65 wt% total organic carbon, and it has around 5 wt% kerogen based on CHNS-O elemental and total organic carbon analysis. The isolated kerogen has high sulfur content due to the remaining pyrite after the kerogen isolation processes, in line with the qualitative XRD analysis. The hydrogen to carbon atom ratio is 0.750 and oxygen to carbon atom ratio is 0.039 in the isolated kerogen, which indicates that the kerogen is Type II [42]. In the organic petrography analysis (Table S4), the shale sample is interpreted to be of marine origin owing to the presence of abundant fluorescing liptinite maceral in the form of lamalginite, degraded lamalginite and amorphinite. Small amounts of vitrinite maceral are present in the sample. The IR analysis shows that aliphatic/aromatic ratio in the shale sample is 1.35.

3.2. Excess adsorption

In a recent paper, we have measured excess adsorption of methane, ethane, propane, *n*-butane, and *i*-butane, and carbon dioxide in an outcrop shale rock (Kimmeridge Blackstone). Eq. (8) was used to estimate absolute adsorption from excess adsorption. The absolute adsorption showed a monotonic increase with pressure. In this work Eq. (8) results in a non-monotonic behavior and casts doubt on its validity.

For the shale samples, the excess sorption isotherms of various hydrocarbons and carbon dioxide at three different temperatures are presented in Fig. 1. The results are based on Eq. (5). The measurements are reproducible (see Fig. S3). In all the sorption plots we divide the amount by the mass of sample. At high temperature, the excess adsorption decreases as expected, because the molecules have higher kinetic energy to escape from the surface. For methane, ethane and carbon dioxide, the results indicate pronounced hysteresis. At lower pressure, hysteresis is not significant for propane, *n*-butane, and *i*-

butane. The excess adsorption isotherms increase monotonically with pressure increase in propane, *n*-butane, and *i*-butane, which are at relatively lower pressure. At high pressure, the excess adsorption of ethane and carbon dioxide decreases significantly as pressure increases, and it shows slight downward trend in methane as well. The relationship between excess adsorption and bulk fluid density can provide insights (see Fig. S4). The details will be discussed in the next section. At 60 °C, the excess adsorption of ethane in shale is negative when the pressure is over 120 bar. Various authors, as we discussed in the introduction, have interpreted the negative excess adsorption differently. In this work, we suggest that the negative excess adsorption is due to two different effects, the accessible volume for different gases and the swelling effect. The model will be discussed in the next section.

For the isolated kerogen, the excess sorption isotherms of various hydrocarbons and carbon dioxide at 60 °C are presented in Fig. 2. The experiments are reproducible as in the shale (see Fig. S5). The excess adsorption in kerogen is much higher than in the shale; it can be up to 10–15 times. The increase is mainly related to the higher surface area and the higher content of nanopores in kerogen.[1] The shape of the plots in kerogen are similar to the shape in shale, which indicates that the adsorption in kerogen and in shale are strongly correlated.

For the isolated kerogen sample, if we assume the adsorption only occurs in the organic carbon, the contribution of kerogen for the entire shale can be estimated from these results based on TOC in shale. Because the isolated kerogen contains some impurities, we should take into account the TOC in kerogen as well. The results show that the contribution of kerogen is over 50% (see Fig. S6), although the TOC is only 3.65% in shale. On the other hand, although kerogen is the dominated component in shale for adsorption, the contribution of inorganic matter cannot be neglected, especially when kerogen content is low.

3.3. Absolute adsorption

The absolute adsorption can be estimated from excess adsorption based on Eq. (8) with the adsorbed layer density approximated by liquid density or Grand Canonical Monte Carlo (GCMC) simulations. The liquid densities at the normal boiling point for hydrocarbons, and at the triple point for carbon dioxide are used in our investigation [29,43]. We have also computed adsorbed layer density from the GCMC simulations in carbon slit pores as a function of pressure [29].

The calculated absolute adsorptions of methane, ethane and carbon dioxide at different temperatures, based on liquid density approximation and estimated density from GCMC simulations, are presented in Fig. 3. Generally, the absolute adsorption increases monotonically with pressure, which is the case for methane. However, there are significant downward trends for ethane and carbon dioxide (see Fig. 3d to i). At high pressure, the absolute adsorption even becomes negative in ethane at 60 °C. The results based on the conventional expression magnifies the negative values indicating the need for an alternative method. The absolute adsorption of methane shows clear difference between the two assumptions of average adsorbed layer densities, while they are almost the same for ethane and carbon dioxide. As mentioned by Zhao et al. [29] the liquid density of methane is not well defined at the temperatures of 60, 90, and 120 °C. The adsorbed layer density of methane from GCMC simulation has a clear foundation.

For propane, *n*-butane, and *i*-butane, the absolute adsorption increase monotonically with pressure increase as well (see Fig. 4). The results also show that the absolute adsorption is very close to the excess adsorption, due to the significant higher adsorbed layer density than the bulk phase at low pressure. The absolute adsorption can be approximated by the excess adsorption at low pressure.

The absolute adsorption data in kerogen at 60 °C are presented in Fig. S7 which have similar trends as the corresponding shale sample. For methane, different adsorbed densities result in significantly different adsorption plots. There is a downward trend in ethane and
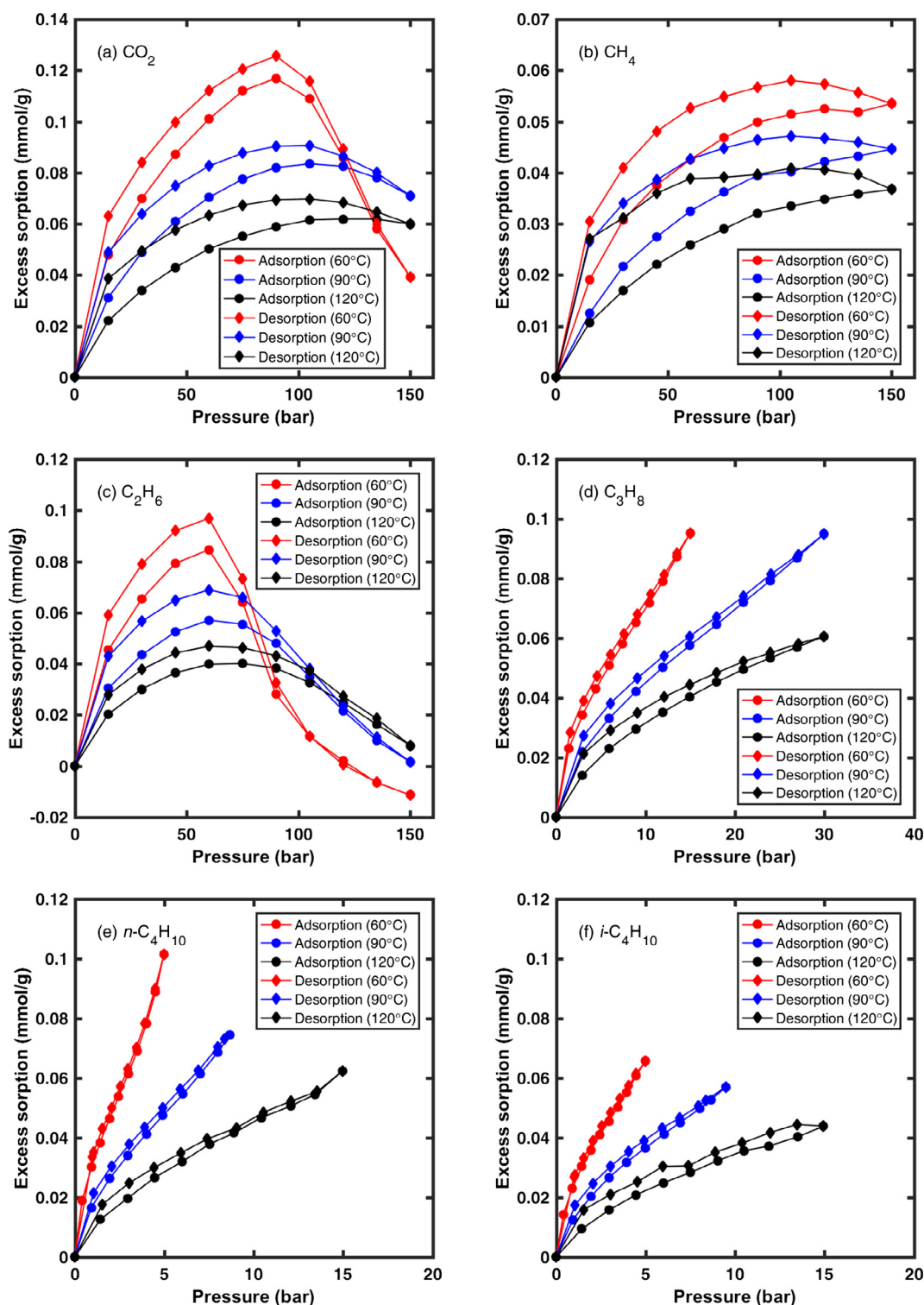
Fig. 1. Excess sorption isotherms of various hydrocarbons and carbon dioxide in shale rock at three different temperatures.

carbon dioxide adsorption. For propane and butanes, the absolute adsorptions and excess adsorptions are close and increase monotonically with pressure.

4. Proposed model

4.1. Adsorbed layer volume

Our proposed model to calculate absolute adsorption from excess adsorption is based on Eq. (6) which requires adsorbed layer volume. In our recent work, we have shown that V^A can be treated as constant in high pressure range based on molecular simulations (see Fig. S8) [29]. In Fig. 5, we present the relationship among excess adsorption, bulk fluid density, and adsorbed layer density. The bulk fluid density obtained from the adsorption measurements in shale are provided in Fig. S9. Generally, both the bulk fluid density and the adsorbed layer density increase as the pressure increases. The excess adsorption strongly correlates with the density difference between the adsorbed layer and
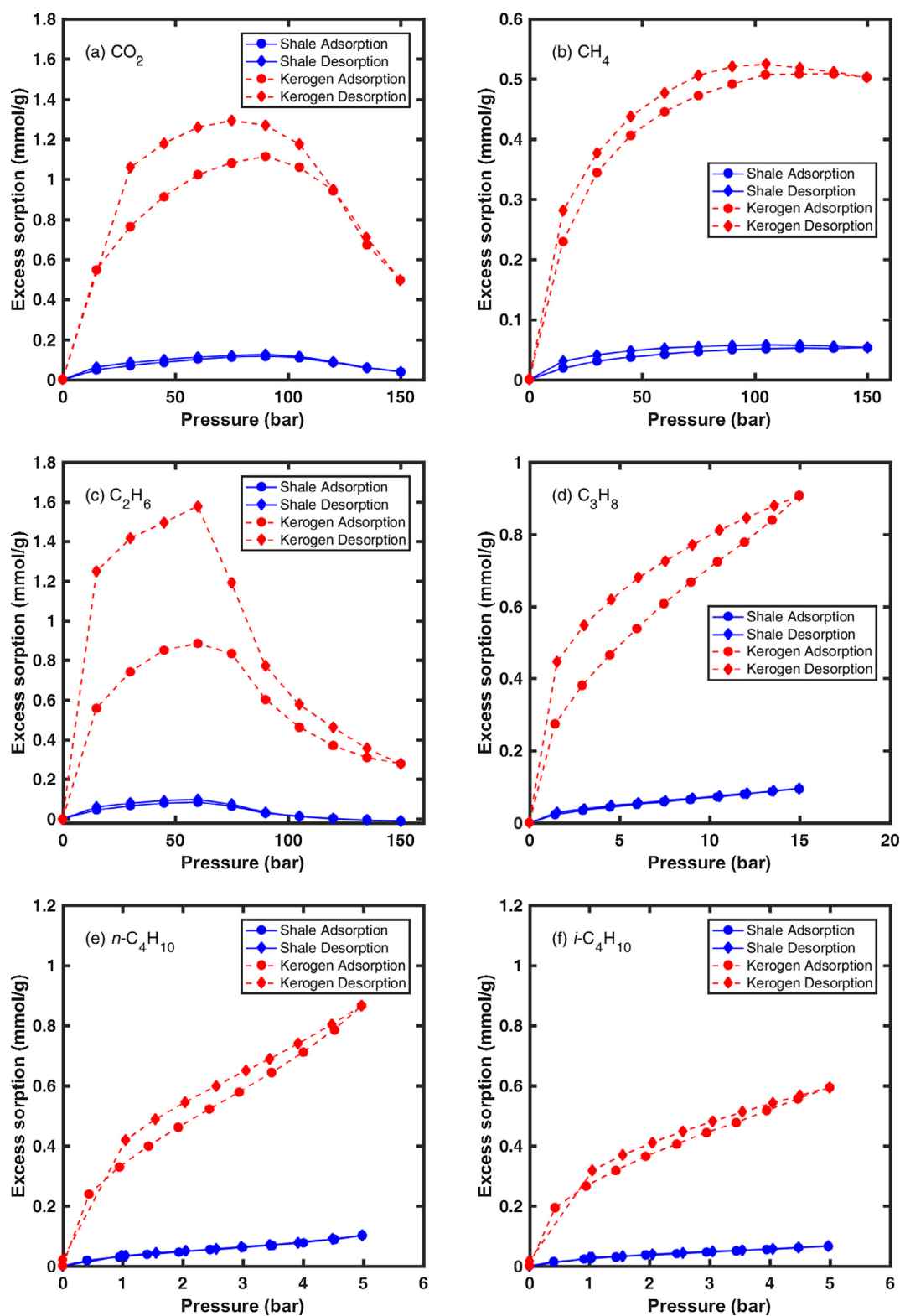
Fig. 2. Excess sorption isotherms of various hydrocarbons and carbon dioxide in isolated kerogen at 60 °C. Excess sorption isotherms in the shale rock are also presented.

the bulk. The results in panels (d) and (f) of Fig. 5 reveal that, with the pressure increase, the adsorbed layer densities have more significant increase than in the bulk at low pressure. However, the adsorbed layer densities of ethane and carbon dioxide do not have a significant change at high pressure, while the bulk fluid densities can increase significantly. When there is a maximal density difference, the excess

adsorption reaches the maximum. Then, the excess adsorption reveals a decreasing trend in ethane and carbon dioxide at high pressure. Because the GCMC results are from carbon slit pores, there are minor deviations between the maximal excess adsorption and the maximal density difference. Fig. 5c, 5e, and S4 show that the excess adsorption develops a linear relationship with bulk fluid density at high pressure in ethane
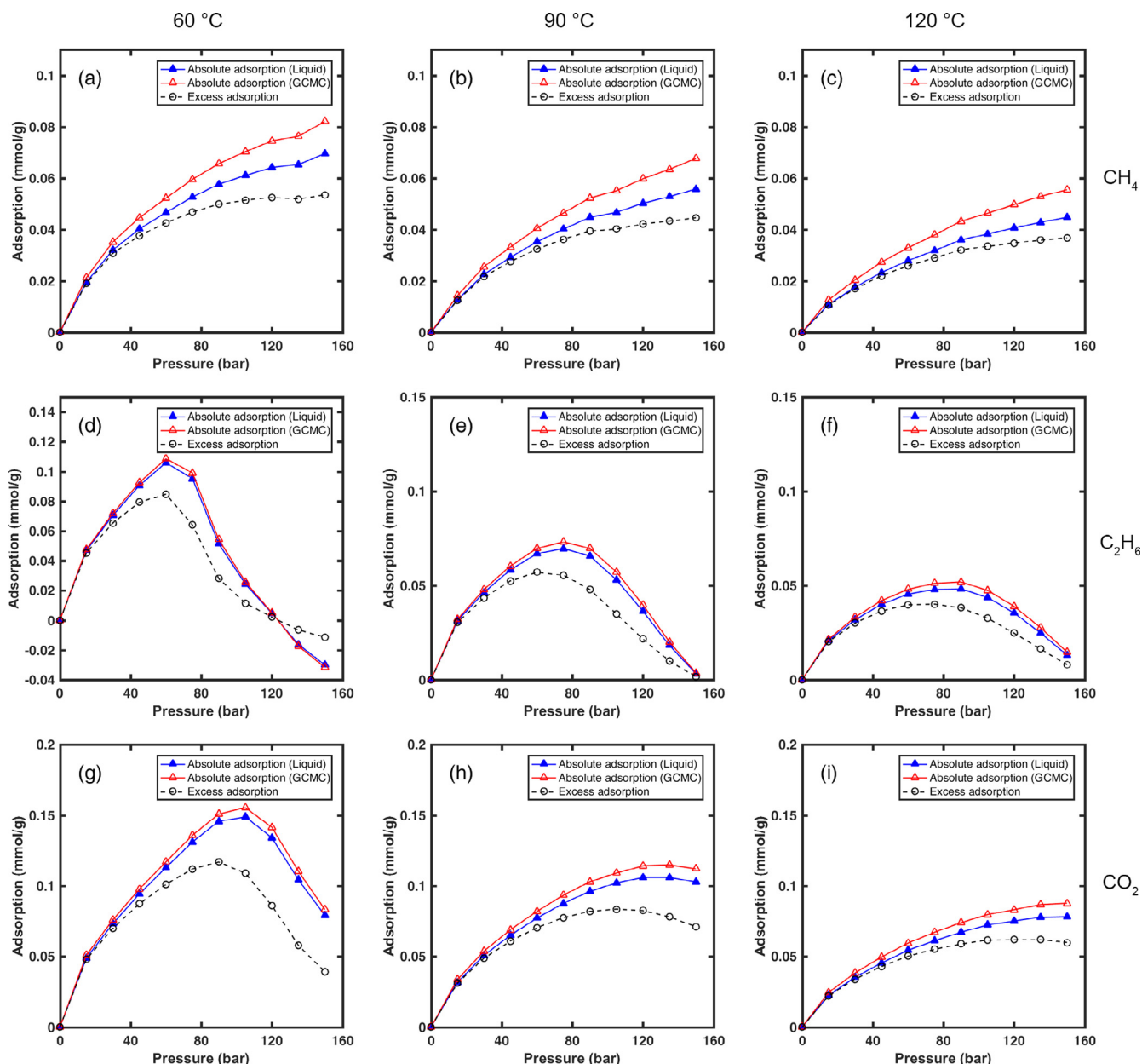
Fig. 3. Absolute adsorption based on conventional model for methane, ethane, and carbon dioxide in shale rock at three different temperatures. The adsorbed layer densities are based on liquid densities and the GCMC simulations in slit pores.

and carbon dioxide. This trend correlates to the condition when the adsorbed layer is almost saturated, and the density reaches a plateau. Unlike ethane and carbon dioxide, methane does not have a constant negative slope in the pressure difference plot below 150 bar.

The differential of Eq. (6) at constant V^A combined with Eq. (7) reads,

$$V^A d\rho^A = dm^E + V^A d\rho^B \qquad (9)$$

The differential of adsorbed layer density can be approximated as zero ($d\rho^A = 0$) at high pressure. Then, the volume of adsorbed layer can be determined from:

$$V^A = -\frac{dm^E}{d\rho^B} \qquad (10)$$

The above expression can be used to compute the adsorbed layer volume. Note that Figs. S4a and S4c give a clear experimental evidence of validity of Eq. (10) to compute the adsorbed layer volume of ethane at 60, 90, and 120 °C, and of carbon dioxide at 60 °C. Because only in

ethane and carbon dioxide there are significant decreasing trends in the absolute adsorption from the conventional approach of Eq. (8), the rest of this work will mainly focus on the analysis of these two gases.

The absolute adsorption of ethane and carbon dioxide are shown in Fig. 6 from the two different models. The conventional model vastly underestimates adsorption of ethane and carbon dioxide, and may magnify the unphysical negative value from excess adsorption. The results from our model show a slight decrease in absolute adsorption at very high pressure, which will be discussed in the next two sections. We will discuss what mechanisms result in the downward trend.

4.2. Accessible pore volume in different gases

In this work and also the work of many authors, the sample volume V^S is obtained from the buoyancy measurement with helium. The kinetic diameters of many measuring gas molecules for adsorption are different from helium [16]. Because of the micropores in shale, the difference of kinetic diameters between the gases can lead to different
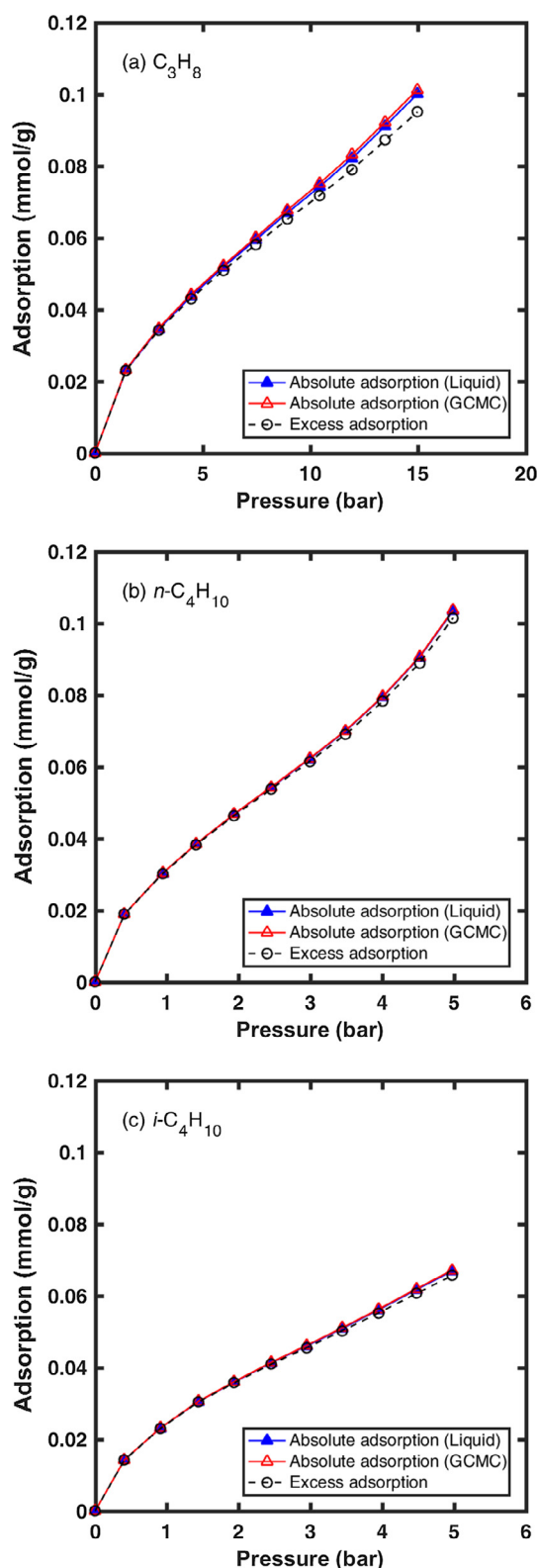
Fig. 4. Absolute adsorption based on conventional model for propane, *n*-butane and *i*-butane in shale at 60 °C. The adsorbed layer densities are based on liquid densities and the GCMC simulations in slit pores.

accessible pore volumes in the sample [16,44]. Fig. 7 is a sketch which shows the effect of molecular size on accessible pore volume. Because helium has the smallest kinetic diameter in this study, it has the largest accessible pore volume (see Fig. 7a). For methane, ethane and other larger molecules, the molecules can be blocked by small pore throats,

e.g. less than 0.38 nm. In the same accessible pore, the effective accessible pore volume can be different for the gases as well. The effect of molecular size can be significant in micropores [16]. The sample volume refers to the sample matrix where the measuring gas cannot access. In the adsorption measurement, the accessible pore volume effect will result in the deviation between the measured sample volume with helium and the actual effective sample volume for the measuring gas. We can include the pore volume that cannot be accessed as part of the rock matrix. The effective sample volume can be defined as

$$V^{S,e} = V^S(1 + \omega) \tag{11}$$

where ω is the relative deviation between the effective sample volume for the measuring gas and the measured sample volume by helium. Based on Eqs. (4), (5), and (11), the absolute adsorption and excess adsorption can be expressed by:

$$m^A = \Delta m - m^{SC} - m^S + [V^{SC} + V^S(1 + \omega) + V^A]\rho^B \tag{12}$$

$$m^E = \Delta m - m^{SC} - m^S + [V^{SC} + V^S(1 + \omega)]\rho^B \tag{13}$$

4.3. Effect of accessible pore volume on absolute adsorption and excess adsorption

The absolute adsorption and excess adsorption in the shale and kerogen samples for ethane and carbon dioxide at 60 °C with the incorporation of the accessible pore volume in our proposed model are presented in Fig. 8. The results for ethane at 90 °C and 120 °C are plotted in Figs. S10 and S11, respectively. The relative deviation ω was set as 0%, 0.5%, 1.0%, and 1.5% to examine the sensitivity. We find that the absolute adsorption and excess adsorption in shale are very sensitive to the effective sample volume, especially at high pressure. Both the absolute adsorption and excess adsorption are higher than the results without incorporation of the change in accessible volume by different molecules. A small relative deviation of sample volume can lead to pronounced change in absolute adsorption, as high as 40% increase of absolute adsorption by 1.5% relative deviation of effective sample volume. The slight downward trend in carbon dioxide can be eliminated. Moreover, the excess adsorption at high pressure becomes positive by taking into account the effective sample volume effect. Theoretically, the effect is more pronounced in the samples with more ultra-micropores (e.g., below 1-nm) and for larger molecules. Then, the absolute and excess adsorption will have much more underestimation without taking into account the accessible pore volume effect.

For the isolated kerogen, both the absolute adsorption and excess adsorption are corrected to higher values (Fig. 8). However, the relative increase is much smaller than the results in shale. This effect is mainly masked by the kerogen's high adsorption capacity in line with the prediction from Ross and Bustin [16]. The absolute adsorption may be underestimated without the accessible pore volume effect, especially for the sample with low adsorption capacity.

4.4. Swelling effect

Swelling due to adsorption in shale has been reported by many authors as stated in the introduction. In the adsorption measurement, the sample volume V^S or effective sample volume $V^{S,e}$ is treated as constant. The volume of kerogen may swell due to the contact with adsorbate molecules [6,19]. This change (ΔV^S) will increase the buoyancy and lead to the underestimate of adsorption, especially at high pressure or in the samples with low adsorption capacity. The effects of swelling and accessible pore volume can be coupled.

A sketch of swelling is presented in Fig. 9. The kerogen in shale can swell from the original volume in Fig. 9a, determined in the buoyancy measurement, to a larger volume $V^{S'}$ in Fig. 9b due to adsorption:
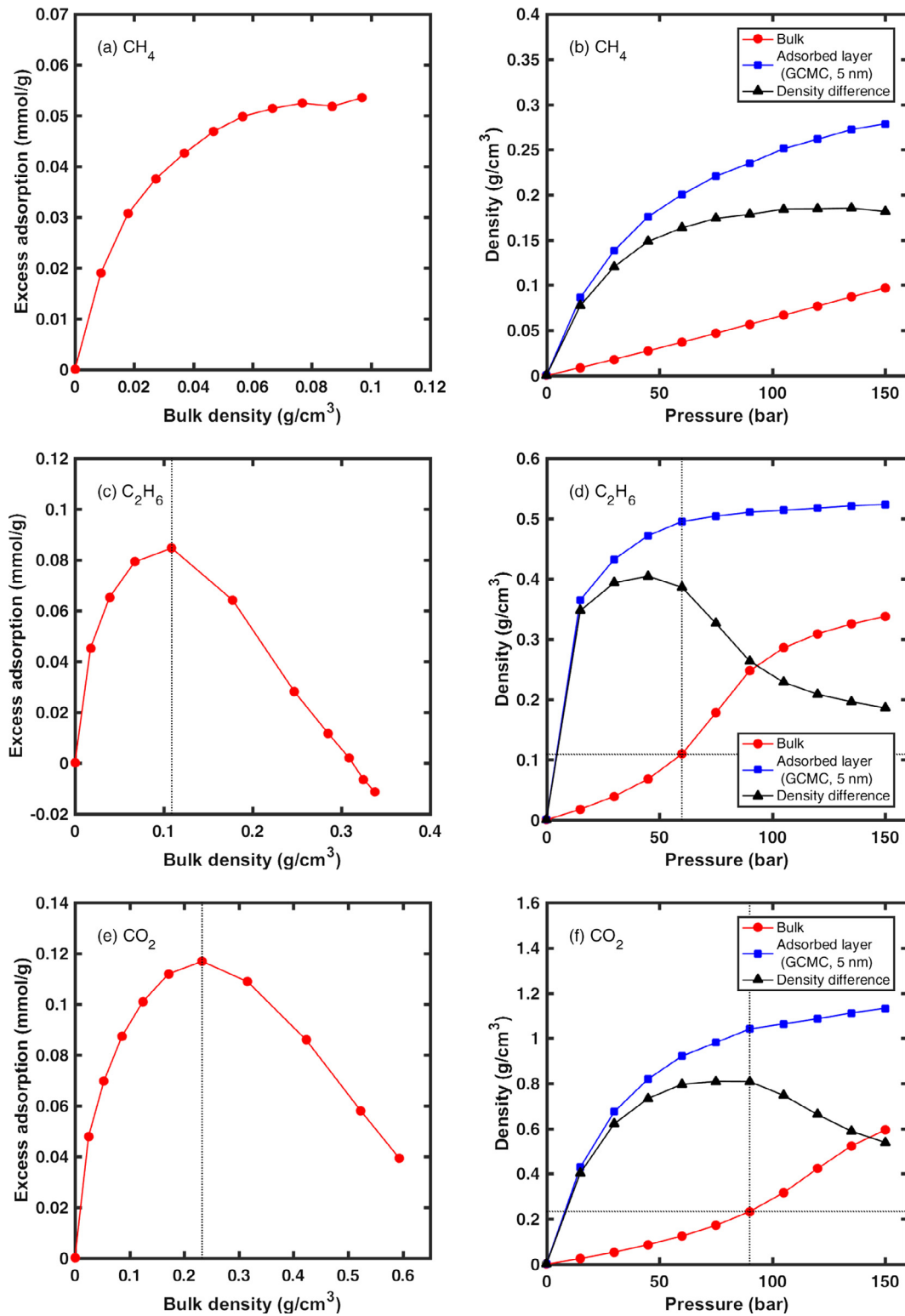
$$V^{S'} = V^{S,e} + \Delta V^S \tag{14}$$

Fig. 5. Excess adsorption, bulk fluid density, and adsorbed layer density of methane, ethane, and carbon dioxide at 60 °C. Excess adsorption vs. bulk fluid density based on the data from experiments (a, c, and e); Bulk fluid density from experiments, adsorbed layer density from GCMC simulations, and the density difference between them (b, d, and f) [29]. The dashed lines are for guiding the eyes to locate the maximum excess adsorption which correlates with pronounced downward in density difference between the adsorbed layer and bulk fluid.

As an analogy to adsorption induced swelling in coal bed methane [45,46], we assume that the volume change due to swelling is proportional to the absolute adsorption amount, which can be expressed as:

$$\Delta V^S = V^{S,e} C \varepsilon^A = V^{S,e} C \varepsilon^{A,\max} \frac{m^A}{m^{A,\max}} \tag{15}$$

where C is the volumetric total organic carbon (TOC) content in shale; ε^A is the adsorption volumetric strain; $\varepsilon^{A,\max}$ and $m^{A,\max}$ are the maximum volumetric strain and maximum adsorption amount,
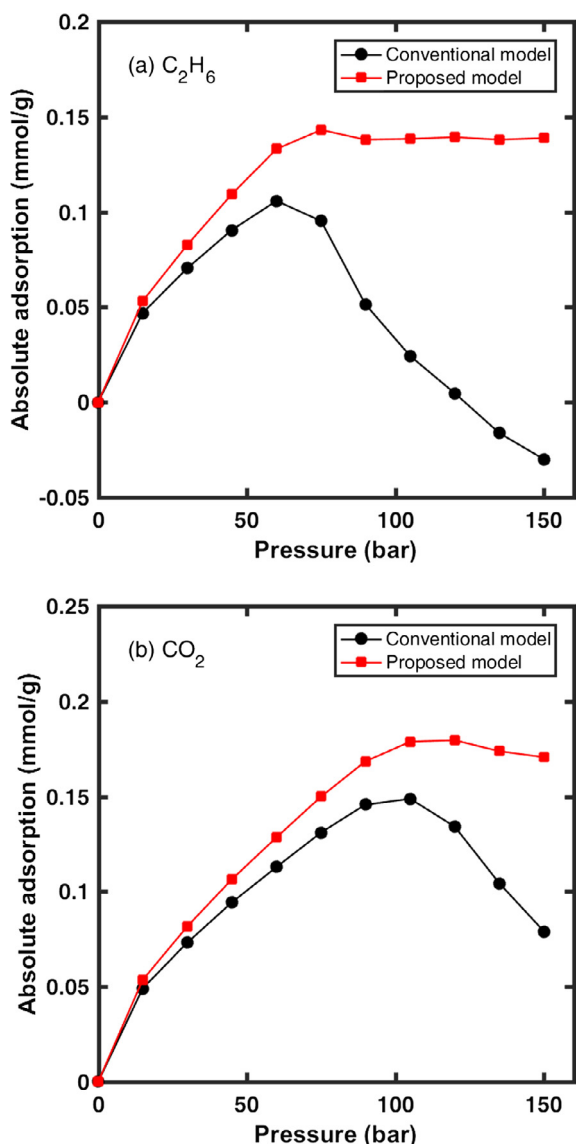
Fig. 6. Absolute adsorption based on the conventional model and the proposed model (without the consideration of accessible pore volume and swelling) for ethane (a) and carbon dioxide (b) at 60 °C. The adsorbed layer densities for conventional method are from liquid densities.

respectively. The maximum adsorption amount is a scaling factor for this relationship, which is assumed to be equal to the maximum adsorbed layer density from GCMC simulation [29]:

$$m^{A,\max} = \rho^{A,\max} V^A \tag{16}$$

The absolute adsorption, when swelling and accessible pore volume are taken into account, can be obtained by combing Eqs. (3) (4), (12), and (14)–(16):

$$m^A = \frac{\Delta m - (m^{SC} + m^S) + \rho^B [V^{SC} + V^S(1 + \omega) + V^A]}{1 - \frac{\rho^B V^S (1 + \omega)}{\rho^{A,\max} V^A} C \varepsilon^{A,\max}} \tag{17}$$

Then, the excess adsorption can be properly calculated based on Eq. (6).

In reservoir simulation and most evaluations, one is interested in the total amount of the fluid in the sample or the reservoir, known as the fluid-in-place (FIP). Fig. 9c and 9d present the sketches of the unconfined and confined conditions for FIP estimation, respectively. In real conditions, the status may be between the two. The unconfined state represents conditions in most laboratory measurements. The confined state represents subsurface conditions.

4.5. Effect of kerogen swelling on absolute adsorption and excess adsorption

The results based on our proposed model with swelling effect for ethane at 60 °C are presented in Fig. 10. The maximum volumetric strain was set as 0%, 5%, and 10% to perform the sensitivity analysis. To examine the sensitivity to swelling alone, the relative deviation ω is set to 0. The absolute adsorption amount is higher when the maximum volumetric strain is higher. As the pressure increases, the absolute adsorption can reach a plateau. The excess adsorption at high pressure becomes positive with consideration of swelling. The results for ethane at 90 °C and 120 °C are presented in Figs. S12 and S13, respectively. For carbon dioxide, there is a slightly downward trend when the swelling effect is weak (see Fig. 10). When the maximum volumetric strain is 10%, the absolute adsorption reaches a plateau. In excess adsorption, the amount will be corrected to higher values when the maximum volumetric strain is higher.

The results for kerogen based on our model are shown in Fig. 11. In ethane and carbon dioxide, when the maximum volumetric strain is higher than 5%, the estimated increase from isolated kerogen is even higher than the total increase in the shale. This indicates that the maximum volumetric strain may be less than 5%. However, in carbon dioxide, when the maximum volumetric strain is less than 5%, the absolute adsorption will have downward trend. It indicates that swelling effect may not be the only mechanism that leads to the downward trend, in which the accessible pore volume effect has to be taken into
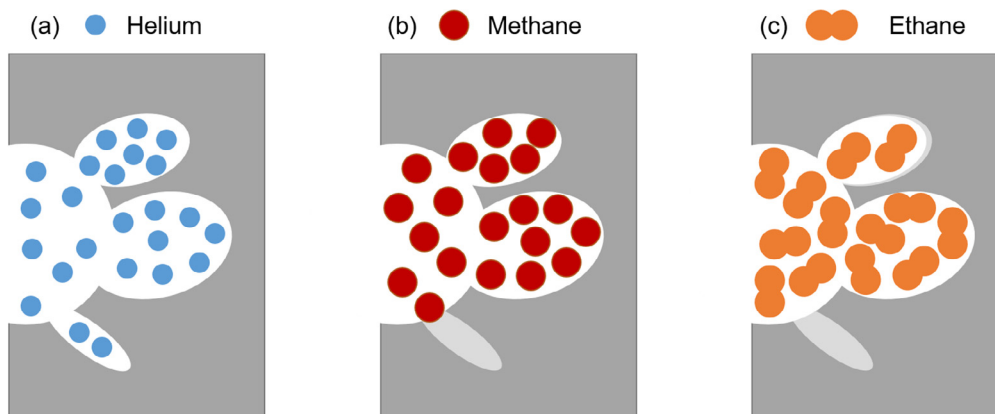

Fig. 7. Sketch of the accessible pore volume and effective sample volume by different gases. The white portion denotes the accessible pore volume. The dark gray portion presents the sample volume measured by helium. The effective sample volume is denoted by the combined portion of dark gray and light gray.
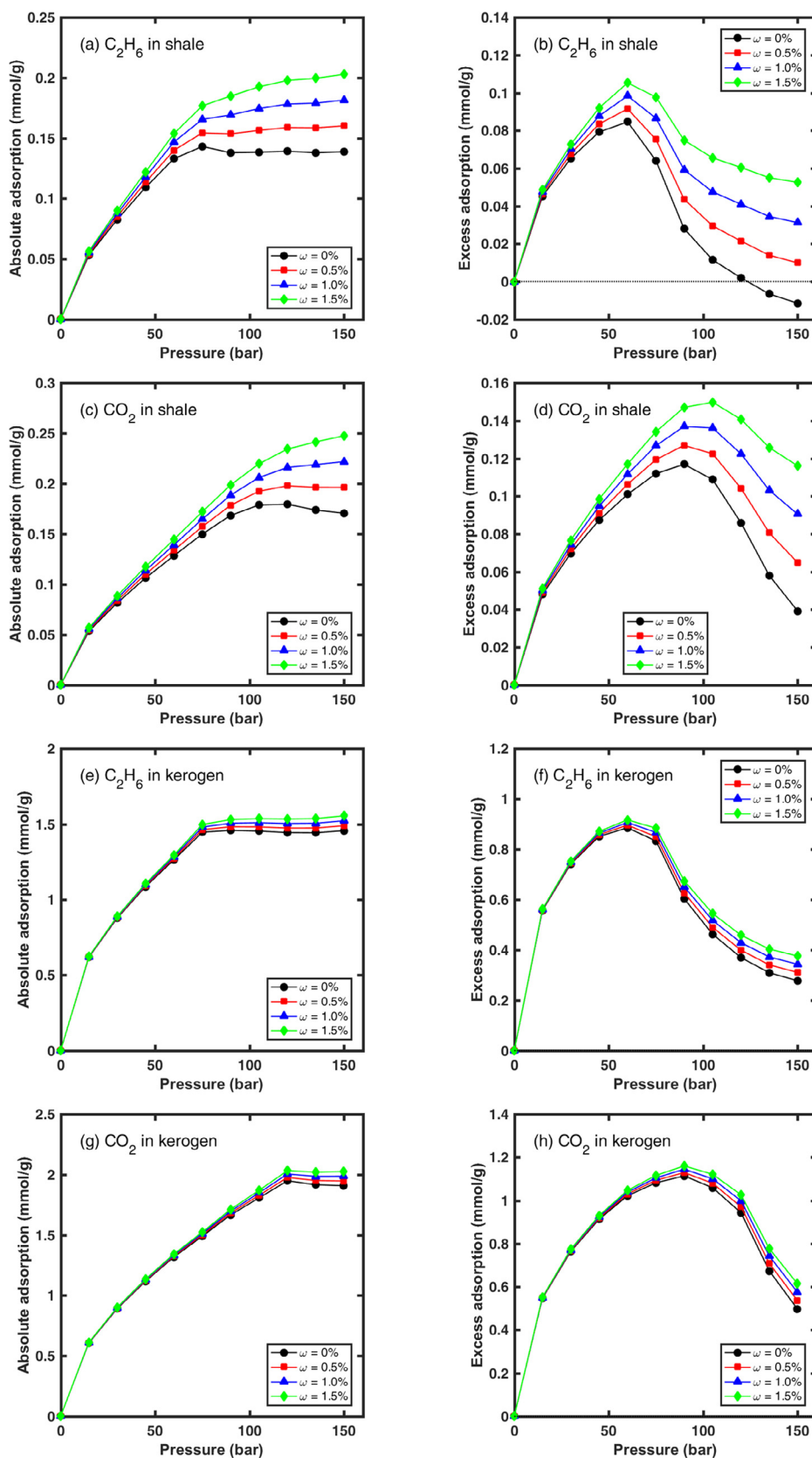
Fig. 8. Absolute adsorption and excess adsorption of ethane and carbon dioxide in the shale rock and kerogen at 60 °C with the effect of accessible pore volume.
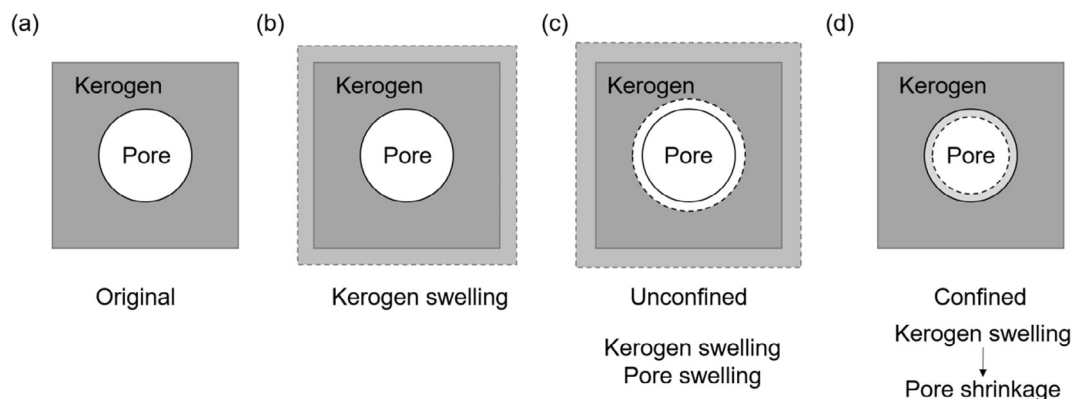
Fig. 9. Sketch of the swelling effect model. The solid line denotes the original state. The dash line represents the status with swelling.

account. In kerogen isolation, the pore structure may change, which can also result in minor deviations.

We provide the results of FIP in both confined and unconfined conditions in the SI (Fig. S14). For the sample in unconfined condition, there would be both the kerogen swelling and the pore expansion. The contribution of pore expansion to FIP increase is comparable to the change of adsorption due to kerogen swelling. The difference in the FIP between the reference case and with 10% maximum volumetric strain

and 10% maximum pore volume change ratio, can be as high as 30% for ethane and 20% for carbon dioxide. For the sample in confined condition, the change will be reduced significantly by these two effects. However, it may have significant effect on permeability [47]. The effects of kerogen swelling and pore shrinkage at in-situ reservoir conditions are more complicated, as they can also be affected by the effective stress.
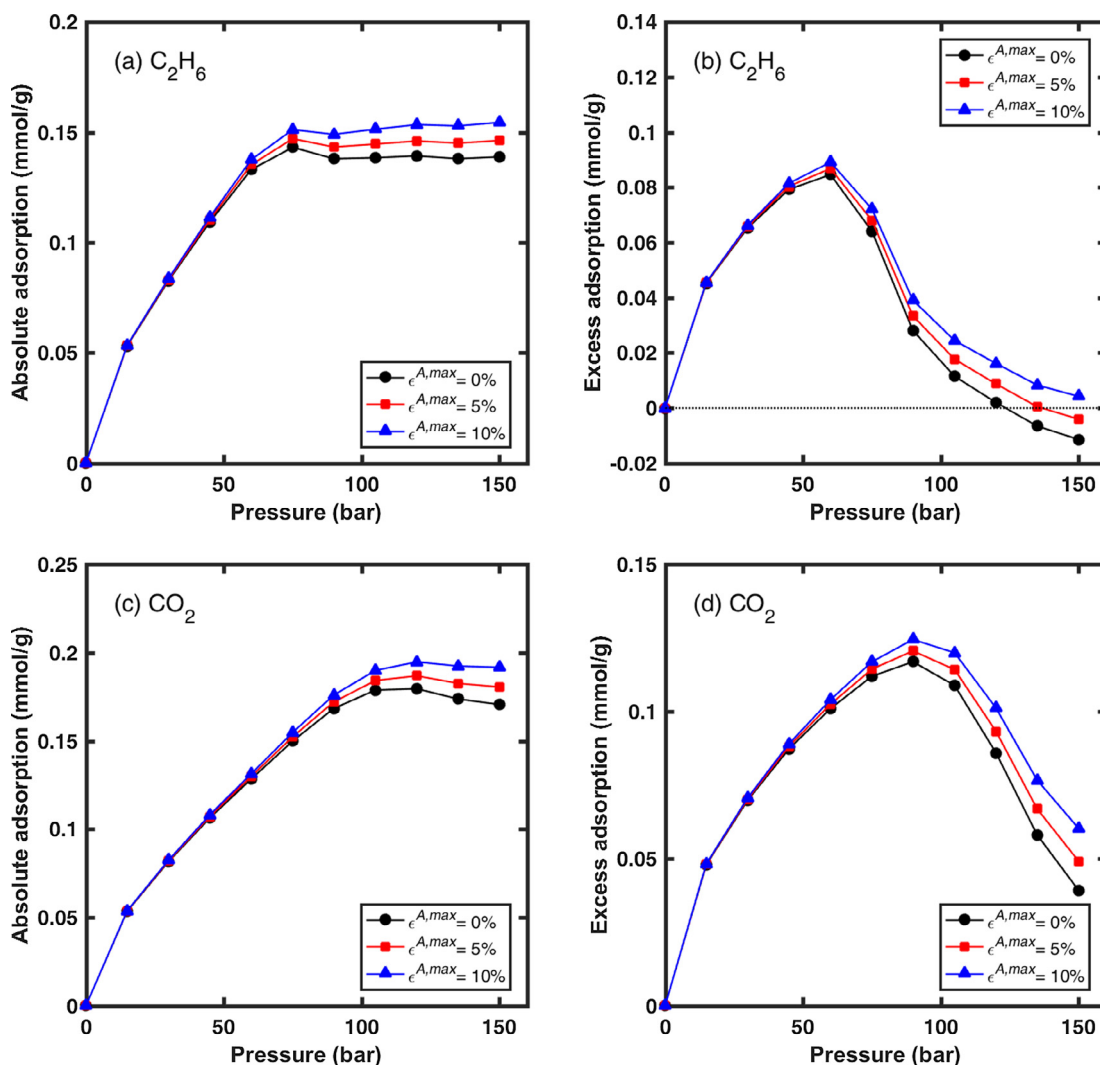

Fig. 10. Absolute adsorption and excess adsorption of ethane and carbon dioxide in the shale rock with swelling effect at 60 °C.
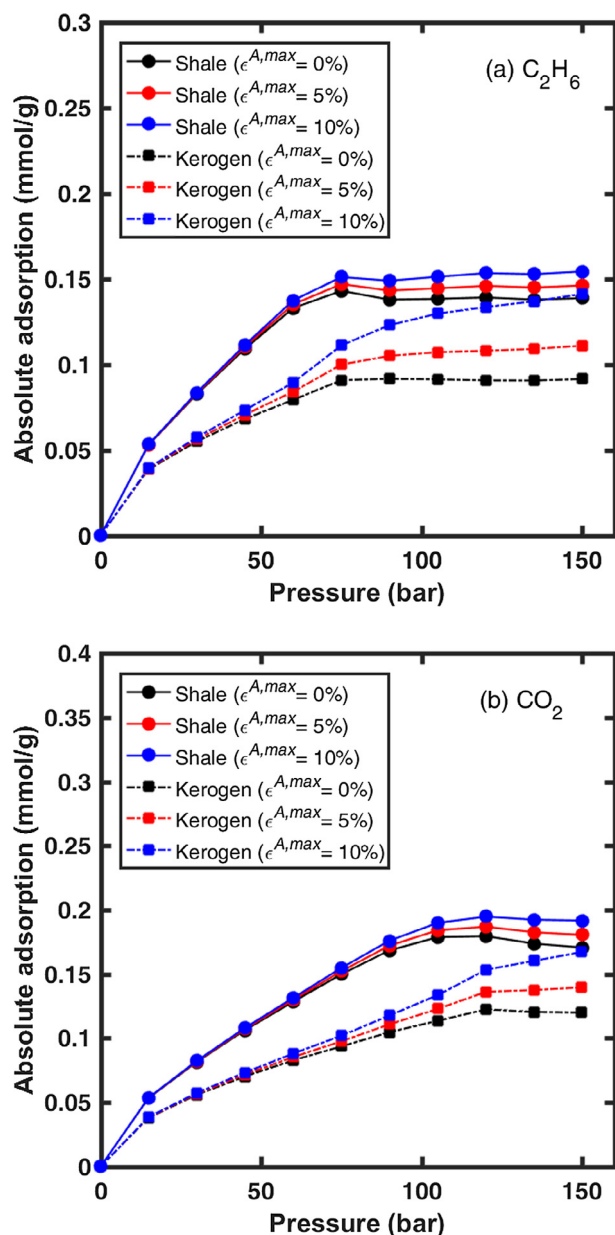
Fig. 11. Absolute adsorption of ethane and carbon dioxide in kerogen and shale rock with swelling effect at 60 °C.

5. Conclusions

The main conclusions drawn from this study are:

1. There is significant sorption hysteresis in ethane and carbon dioxide in the subsurface shale rock with 3.5 wt% TOC to a pressure of 150 bar at the temperatures of 60, 90, and 120 °C. There is also pronounced hysteresis in the isolated kerogen from the shale rock. Ethane shows the highest hysteresis. Methane shows less hysteresis than the other two gases. The sorption hysteresis for propane, *n*-butane, and *i*-butane is not pronounced at low and moderate pressure range of our measurements.

2. At high pressure, the excess adsorption of ethane and carbon dioxide decreases significantly as pressure increases, and there is a slightly downward trend in methane as well. The excess adsorption at high pressure for ethane in shale rock is negative at 60 °C.

3. We offer a clear explanation of the downward trend in terms of the density difference between bulk fluid and adsorbed layer. At low

pressure, the adsorbed layer densities have more significant increase than in the bulk. At high pressure, the adsorbed layer densities do not have a significant change, while the bulk fluid densities can increase significantly. When there is a maximal density difference, the excess adsorption reaches the maximum. Then, the excess adsorption reveals a decreasing trend in ethane and carbon dioxide at high pressure.

4. The excess adsorption in isolated kerogen is 10 to 15 times higher than in the shale. The increase mainly correlates with the higher surface area and the higher content of nanopores in kerogen. The contribution of kerogen in our shale sample is over 50 wt%, although the TOC is only 3.65 wt%. Sorption is dominated by kerogen but the contribution of inorganic matter cannot be neglected.

5. In propane, *n*-butane, and *i*-butane, the absolute adsorption is close to the excess adsorption at mild pressure conditions.

6. The conventional model (based on adsorbed layer density) for the calculation of absolute adsorption may become very unreliable at high pressure.

7. In our proposed model for the absolute adsorption estimation, a key parameter is the volume of the adsorbed layer which can be calculated for the excess adsorption data at high pressure.

8. The accessible pore volume and swelling can affect both absolute and excess adsorption. These parameters will prevent downward trend in absolute adsorption when the pressure increases. The negative excess adsorption at high pressure can be due to these two effects.

Appendix A. Supplementary data

Supplementary data associated with this article can be found, in the online version, at https://doi.org/10.1016/j.fuel.2018.08.023.

References

[1] Wu T, Li X, Zhao J, Zhang D. Multiscale pore structure and its effect on gas transport in organic-rich shale. Water Resour Res 2017;53(7):5438–50.

[2] Li T, Tian H, Xiao X, Cheng P, Zhou Q, Wei Q. Geochemical characterization and methane adsorption capacity of overmature organic-rich Lower Cambrian shales in northeast Guizhou region, southwest China. Mar Pet Geol 2017;86:858–73.

[3] Vandenbroucke M, Largeau C. Kerogen origin, evolution and structure. Org Geochem 2007;38(5):719–833.

[4] Ambrose RJ, Hartman RC, Diaz-Campos M, Akkutlu IY, Sondergeld CH. Shale gas-in-place calculations part I: new pore-scale considerations. SPE J 2012;17(01):219–29.

[5] Belmabkhout Y, Frere M, De G. Weireld High-pressure adsorption measurements. A comparative study of the volumetric and gravimetric methods. Meas Sci Technol 2004;15(5):848–58.

[6] Heller R, Zoback M. Adsorption of methane and carbon dioxide on gas shale and pure mineral samples. J Unconventional Oil Gas Res 2014;8:14–24.

[7] Gasparik M, Gensterblum Y, Ghanizadeh A, Weniger P, Krooss BM. High-pressure/high-temperature methane-sorption measurements on carbonaceous shales by the manometric method: experimental and data-evaluation considerations for improved accuracy. SPE J 2015;20(04):790–809.

[8] Gasparik M, Ghanizadeh A, Bertier P, Gensterblum Y, Bouw S, Kroos BM. High-pressure methane sorption isotherms of black shales from the Netherlands. Energy Fuels 2012;26(8):4995–5004.

[9] Gasparik M, Bertier P, Gensterblum Y, Ghanizadeh A, Krooss BM, Littke R. Geological controls on the methane storage capacity in organic-rich shales. Int J Coal Geol 2014;123:34–51.

[10] Pan L, Xiao X, Tian H, Zhou Q, Cheng P. Geological models of gas in place of the Longmaxi shale in Southeast Chongqing, South China. Mar Pet Geol 2016;73:433–44.

[11] Zhao H, Lai Z, Firoozabadi A. Sorption hysteresis of light hydrocarbons and carbon dioxide in shales and kerogens. Sci Rep 2017;7(1):16209.

[12] Rexer TF, Mathia EJ, Aplin AC, Thomas KM. High-pressure methane adsorption and characterization of pores in Posidonia shales and isolated kerogens. Energy Fuels

2014;28(5):2886–901.

[13] Zhang J, Clennell MB, Liu K, Pervukhina M, Chen G, Dewhurst DN. Methane and carbon dioxide adsorption on illite. Energy Fuels 2016;30(12):10643–52.

[14] Tian Y, Yan C, Jin Z. Characterization of methane excess and absolute adsorption in various clay nanopores from molecular simulation. Sci Rep 2017;7(1):12040.

[15] Gasparik M, Rexer TF, Aplin AC, Billemont P, De Weireld G, Gensterblum Y, et al. First international inter-laboratory comparison of high-pressure CH4, CO2 and C2H6 sorption isotherms on carbonaceous shales. Int J Coal Geol 2014;132:131–46.

[16] Ross DJ, Bustin RM. Impact of mass balance calculations on adsorption capacities in microporous shale gas reservoirs. Fuel 2007;86(17):2696–706.

[17] Bv Krooss, Van Bergen F, Gensterblum Y, Siemons N, Pagnier H, David P. High-pressure methane and carbon dioxide adsorption on dry and moisture-equilibrated Pennsylvanian coals. Int J Coal Geol 2002;51(2):69–92.

[18] Etminan SR, Javadpour F, Maini BB, Chen Z. Measurement of gas storage processes in shale and of the molecular diffusion coefficient in kerogen. Int J Coal Geol 2014;123:10–9.

[19] Chen T, Feng X-T, Pan Z. Experimental study of swelling of organic rich shale in methane. Int J Coal Geol 2015;150:64–73.

[20] Savest N, Oja V, Kaevand T, Lille Ü. Interaction of Estonian kukersite with organic solvents: A volumetric swelling and molecular simulation study. Fuel 2007;86(1):17–21.

[21] Kelemen S, Kwiatek L, Siskin M, Lee A. Structural response of coal to drying and pentane sorption. Energy Fuels 2006;20(1):205–13.

[22] Larsen JW, Li S. An initial comparison of the interactions of Type I and III kerogens with organic liquids. Org Geochem 1997;26(5–6):305–9.

[23] Larsen JW, Li S. Solvent swelling studies of Green River kerogen. Energy Fuels 1994;8(4):932–6.

[24] Ballice L. Solvent swelling studies of Göynük (Kerogen Type-I) and Beypazarı oil shales (Kerogen Type-II). Fuel 2003;82(11):1317–21.

[25] Pathak M, Kweon H, Deo M, Huang H. Kerogen swelling and confinement: its implication on fluid thermodynamic properties in shales. Sci Rep 2017;7(1):12530.

[26] Yang S, Wu W, Xu J, Ji D, Chen Z. Volume effects on methane-shale adsorption under reservoir conditions. In: SPE Europec featured at 78th EAGE Conference and Exhibition. Vienna, Austria; 2016.

[27] Hogg S. Geology and hydrocarbon potential of the Neuquén Basin. J Pet Geol 1993;16(4):383–96.

[28] Horvath Z, Jackson K. Procedure for the Isolation of Kerogen from Sedimentary Rocks. Bureau of Mineral Resources, Geology and Geophysics; 1981.

[29] Zhao H, Wu T, Firoozabadi A. High pressure sorption of various hydrocarbons and carbon dioxide in Kimmeridge Blackstone and isolated kerogen. Fuel 2018;224:412–23.

[30] Rexer TF, Benham MJ, Aplin AC, Thomas KM. Methane adsorption on shale under simulated geological temperature and pressure conditions. Energy Fuels 2013;27(6):3099–109.

[31] Payne H, Sturdevant G, Leland T. Improved two-dimensional equation of state to predict adsorption of pure and mixed hydrocarbons. Ind Eng Chem Fundam 1968;7(3):363–74.

[32] Furukawa H, Miller MA, Yaghi OM. Independent verification of the saturation hydrogen uptake in MOF-177 and establishment of a benchmark for hydrogen adsorption in metal–organic frameworks. J Mater Chem 2007;17(30):3197–204.

[33] Neimark AV, Ravikovitch PI. Calibration of pore volume in adsorption experiments and theoretical models. Langmuir 1997;13(19):5148–60.

[34] Dubinin M. The potential theory of adsorption of gases and vapors for adsorbents with energetically nonuniform surfaces. Chem Rev 1960;60(2):235–41.

[35] Aljamaan H, Al Ismail M, Kovscek AR. Experimental investigation and Grand Canonical Monte Carlo simulation of gas shale adsorption from the macro to the nano scale. J Nat Gas Sci Eng 2016;48:119–37.

[36] Ozawa S, Kusumi S, Ogino Y. Physical adsorption of gases at high pressure. IV. An improvement of the Dubinin—Astakhov adsorption equation. J Colloid Interface Sci 1976;56(1):83–91.

[37] Tsai M, Chen W, Cen P, Yang R, Kornosky R, Holcombe N, et al. Adsorption of gas mixture on activated carbon. Carbon 1985;23(2):167–73.

[38] Liang L, Luo D, Liu X, Xiong J. Experimental study on the wettability and adsorption characteristics of Longmaxi Formation shale in the Sichuan Basin, China. J Nat Gas Sci Eng 2016;33:1107–18.

[39] Yang F, Ning Z, Zhang R, Zhao H, Krooss BM. Investigations on the methane sorption capacity of marine shales from Sichuan Basin, China. Int J Coal Geol 2015;146:104–17.

[40] Wang Y, Zhu Y, Liu S, Zhang R. Methane adsorption measurements and modeling for organic-rich marine shale samples. Fuel 2016;172:301–9.

[41] Sakurovs R, Day S, Weir S, Duffy G. Application of a modified Dubinin−Radushkevich equation to adsorption of gases by coals under supercritical conditions. Energy Fuels 2007;21(2):992–7.

[42] Peters KE, Moldowan JM. The biomarker guide: interpreting molecular fossils in petroleum and ancient sediments. 2nd ed. Englewood Cliffs, NJ, United States: Prentice Hall; 1993.

[43] Linstrom P, Mallard W. NIST chemistry webbook; NIST standard reference database No. 69; 2010. http://webbook.nist.gov/chemistry/ [accessed 1 July 2017].

[44] Collell J, Ungerer P, Galliero G, Yiannourakou M, Fo Montel, Pujol M. Molecular simulation of bulk organic matter in type II shales in the middle of the oil formation window. Energy Fuels 2014;28(12):7457–66.

[45] Cui X, Bustin RM, Chikatamarla L. Adsorption-induced coal swelling and stress: Implications for methane production and acid gas sequestration into coal seams. J Geophys Res Solid Earth 2007;112(B10):B10202.

[46] Pini R, Ottiger S, Burlini L, Storti G, Mazzotti M. Role of adsorption and swelling on the dynamics of gas injection in coal. J Geophys Res Solid Earth 2009;114(B4):B04203.

[47] Kumar H, Elsworth D, Mathews J, Marone C. Permeability evolution in sorbing media: analogies between organic-rich shale and coal. Geofluids 2016;16(1):43–55.